Supplementary Information (SI) for Energy & Environmental Science.
This journal is © The Royal Society of Chemistry 2024

Supporting Information

Simultaneously Improving the Efficiencies of Organic Photovoltaic Devices and Modules by Finely Manipulating the Aggregation Behaviors of Y-Serie Molecules

Yaohui Li, Ziyan Jia, Peihao Huang, Chuanlin Gao, Yufei Wang*, Shuangxi Xue, Shirong Lu*, Yang (Michael) Yang

Materials

PEDOT:PSS (Clevios P VP Al 4083) was purchased from Xi'an P-OLED Technology Co Ltd. PM6, D18, Y6, BTP-ec9 and L8BO were purchased from Solarmer Materials Ins. PNDIT-F3N was purchased from eFlexPV Limited (China). 1,1,2,2-Tetrabromoethane (2Br) was purchased from Sigma-Aldrich Trading Co Ltd. All materials were used as received without additional purification. ITO substrate (sheet resistance of 15 Ω sq^{-1}) was purchased from South China Xiang Science & Technology Company Limited.

Small-Area Device Fabrication

OPV devices with traditional structure of ITO/PEDOT:PSS/active layer/PNDIT-F3N/Ag were fabricated. The ITO substrate was thoroughly cleaned with deionized water, acetone and alcohol, followed by UV-ozone treatment for 25 min. PEDOT:PSS aqueous solution was filtered using a 0.45 μm polyether sulfone filter (Jinteng company). PEDOT:PSS was spin-coated onto as-precleaned ITO and then baked at 150 °C for 15 min. The mixed PM6:Y6, PM6:BTP-eC9, and PM6:L8-BO with the same D:A ratio of 1:1.2 were dissolved in chloroform solvent at a donor concentration of 7.5 mg mL^{-1}. The mixed PM6:D18:L8-BO with a D:A ratio of 0.8:0.2:1.2 was dissolved in chloroform solvent at a donor concentration of 6.5 mg mL^{-1}. Before spin-coating the active layer, solvent additive was added to active layer solution. The active layer solution was spin-coated on the PEDOT:PSS and then thermally annealed at 75°C for 5 min. A ~5 nm PNDITF3N film was spin-coated on the top of the active layer. Then, Ag was thermally evaporated under a pressure of 3.3×10^{-4} Pa.

Large-Area Device Fabrication

The pre-deposited ITO substrate was scribed by a 1064 nm nano-sec laser beam (2 W) to form an isolated ITO unites (P1 scribing, see Fig. 4e). After cleaning, PEDOT:PSS layer, PM6:D18:L8BO with 2Br layer and PNDIT-F3N layer were sequentially deposited onto ITO substrate in the same way as the small area device. Next, the stacked layer was scribed by another 532nm nano-sec laser beam (P2 scribing). Ag electrode was thermally deposited under a pressure of 3.3×10^{-4} Pa. P3 scribing (532nm nano-sec laser beam) was carried out to form a series of sub-cells. The geometric fill factor (GFF) of the module is 97.0%. The module area used to measure the PCE was defined by the aperture mask as 19.3 cm^2.

Measurement and Characterization

UV-vis absorption spectrum was measured by Carry 7000 spectrophotometer (Agilient). The sample films for UV-vis absorption measurements were prepared on quartz substrates. FTIR spectra was measured by Spectrum Two spectrometer (Perkin

Eimer). TGA tests was measured by thermo gravimetric analyzer (Mettler Toledo) at 1℃/min. AFM measurement was measured by using Dimension Icon atomic force microscopy (Bruker) with the tapping mode. GIWAXS measurement was measured by the Xeuss 2.0 SAXS with a Cu X-ray source (8.05 keV). The sample films for GIWAXS measurement were deposited on the Si substrate. TEM measurement was measured by jem-2100 plus system (JEOL). *J–V* curve was measured by Keithley 2400 source meter under AM1.5G light (100 mW cm^{-2}). The light was simulated by the xenon arc lamp of a Class A solar simulator. Light intensity was calibrated by a Newport-calibrated mono crystalline Si diode. EQE spectrum was measured by QR-R system (Enlitech).

DFT Calculations

The molecular packing geometries and electronic properties are calculated by Gaussian 16 with B3LYP-D3BJ functional and 6-311G(d,p) basis sets, where the long alkyl side chains are simplified to methyl groups to construct the molecular models. The possible structures of the complex are generated by Molclus software and are then fully optimized. The optimized geometries don't show any imaginary frequencies. The electronic coupling (transfer integral) for the nearest-neighbor dimers is calculated using the site energy correction method.

SCLC Measurement

The carrier mobilities were measured by fitting the dark current density with the Mott–Gurney law, which is described by the equation of $J = 9\varepsilon_0\varepsilon_r\mu V^2/8L^3$, where J is the current density, ε_0 and ε_r are the vacuum permittivity and the relative permittivity of active layer, respectively, V is the effective voltage and L is the thickness of active layer. Hole-only device configuration: ITO/PEODT:PSS/PM6:Y6 without and with 2Br/MoO_3/Ag and electron-only device configuration: ITO/ZnO/PM6:Y6 without and with 2Br/PNDITF3N/Ag.

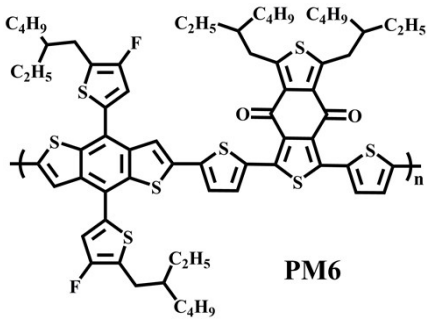

Figure S1. The chemical structure of PM6.

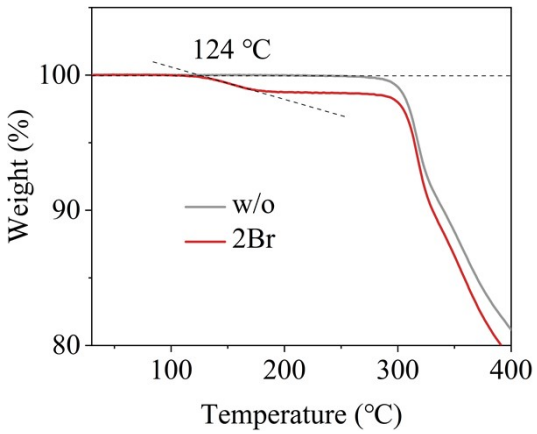

Figure S2. TGA plot of PM6:Y6 film without and with 2Br at a heating rate of 1°C/min.

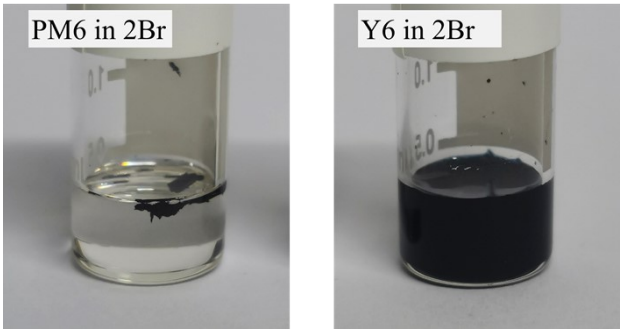

Figure S3. The solubility of PM6 and Y6 in solvent additive 2Br.

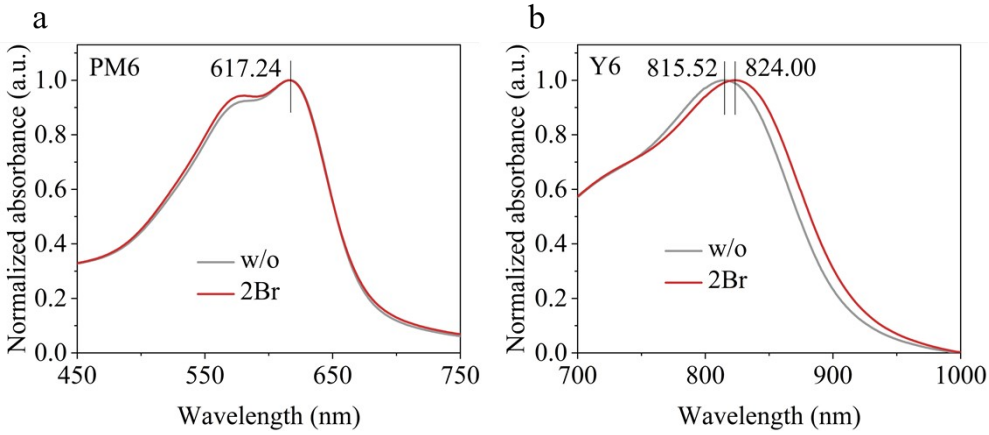

Figure S4. Normalized absorption spectra of PM6 and Y6 film without and with 2Br.

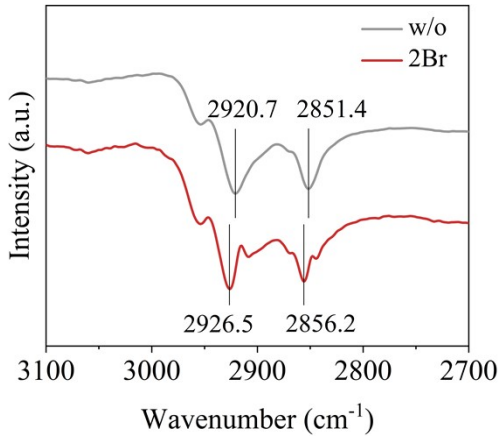

Figure S5. FTIR spectra of pristine Y6 and 2Br-processed Y6.

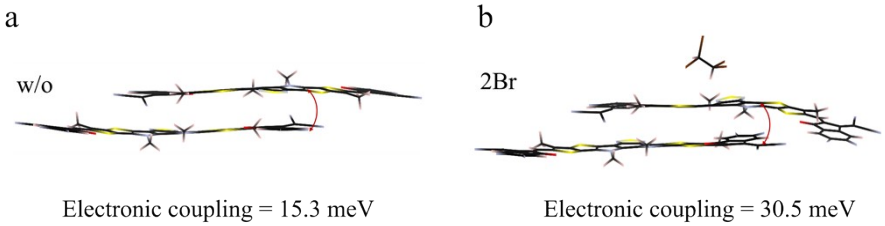

Figure S6. Electronic coupling sketch of Y6 molecular dimer without and with 2Br.

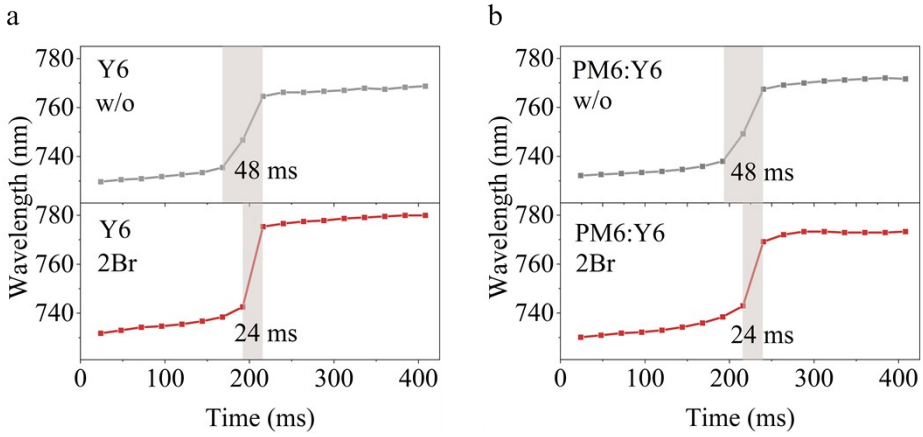

Figure S7. Time evolution of peak position of (a) Y6 and (b) PM6:Y6 without and with 2Br.

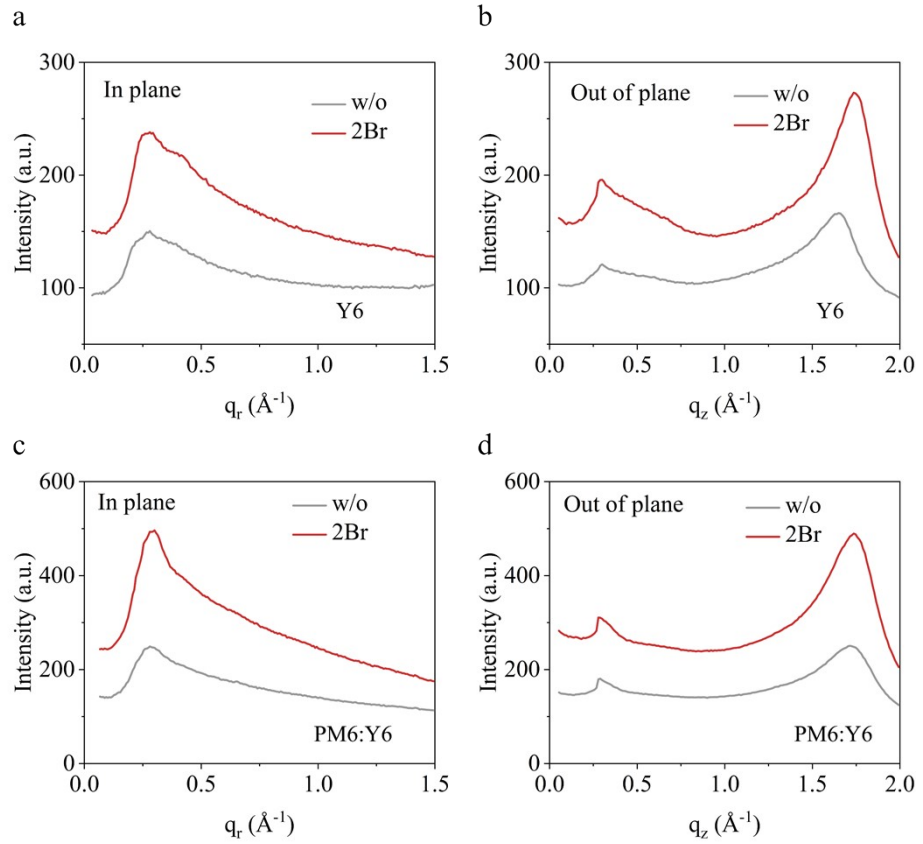

Figure S8. (a) The IP and (b) OOP line-cut profiles of pristine Y6 and 2Br-processed Y6. (c) The IP and (d) OOP line-cut profiles of pristine PM6:Y6 and 2Br-processed PM6:Y6.

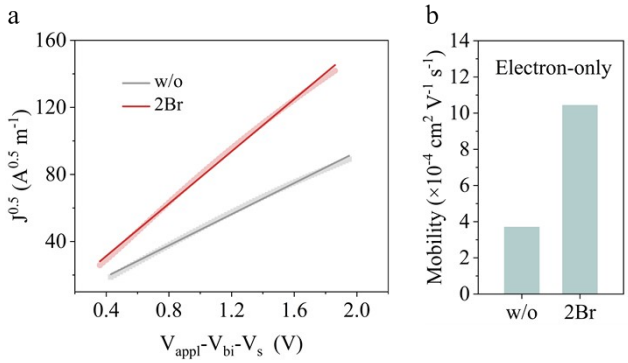

Figure S9. (a) Electron mobilities of pristine Y6 and 2Br-processed Y6. (b) The histogram of mobilities.

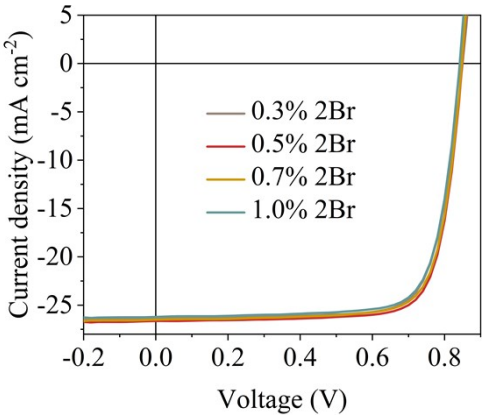

Figure S10. *J-V* curves of PM6:Y6 with different contents of additive 2Br.

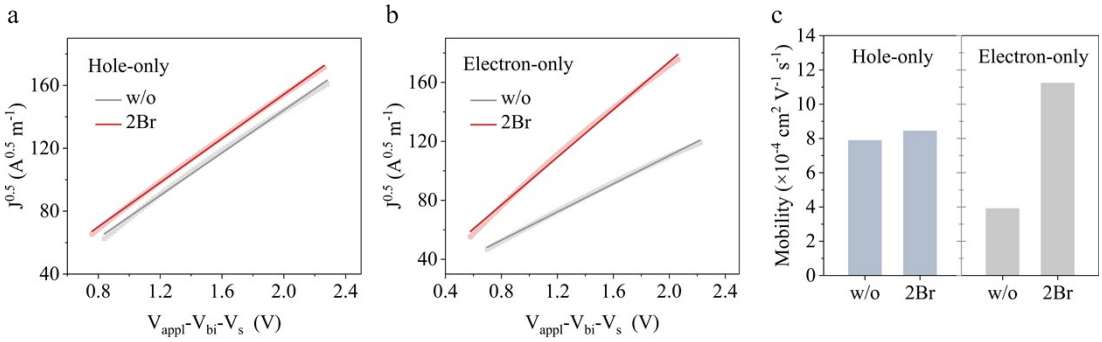

Figure S11. (a) The hole and (b) electron mobilities of pristine PM6:Y6 and 2Br-processed PM6:Y6. (c) The histogram of hole and electron mobilities.

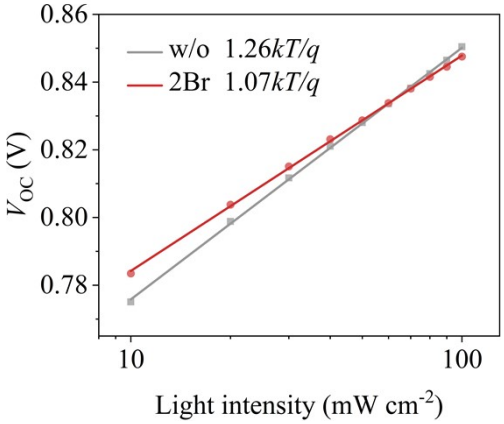

Figure S12. The dependence of V_{oc} as light intensity of pristine PM6:Y6 and 2Br-processed PM6:Y6.

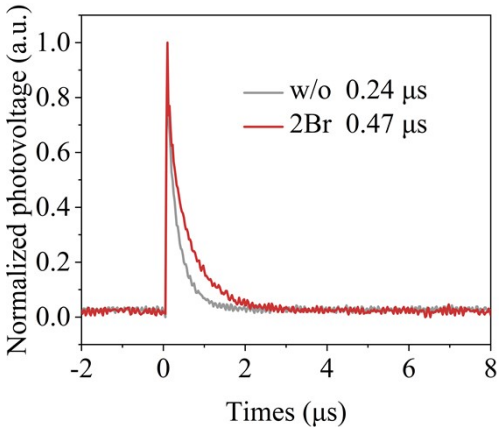

Figure S13. TPV curves of pristine PM6:Y6 and 2Br-processed PM6:Y6.

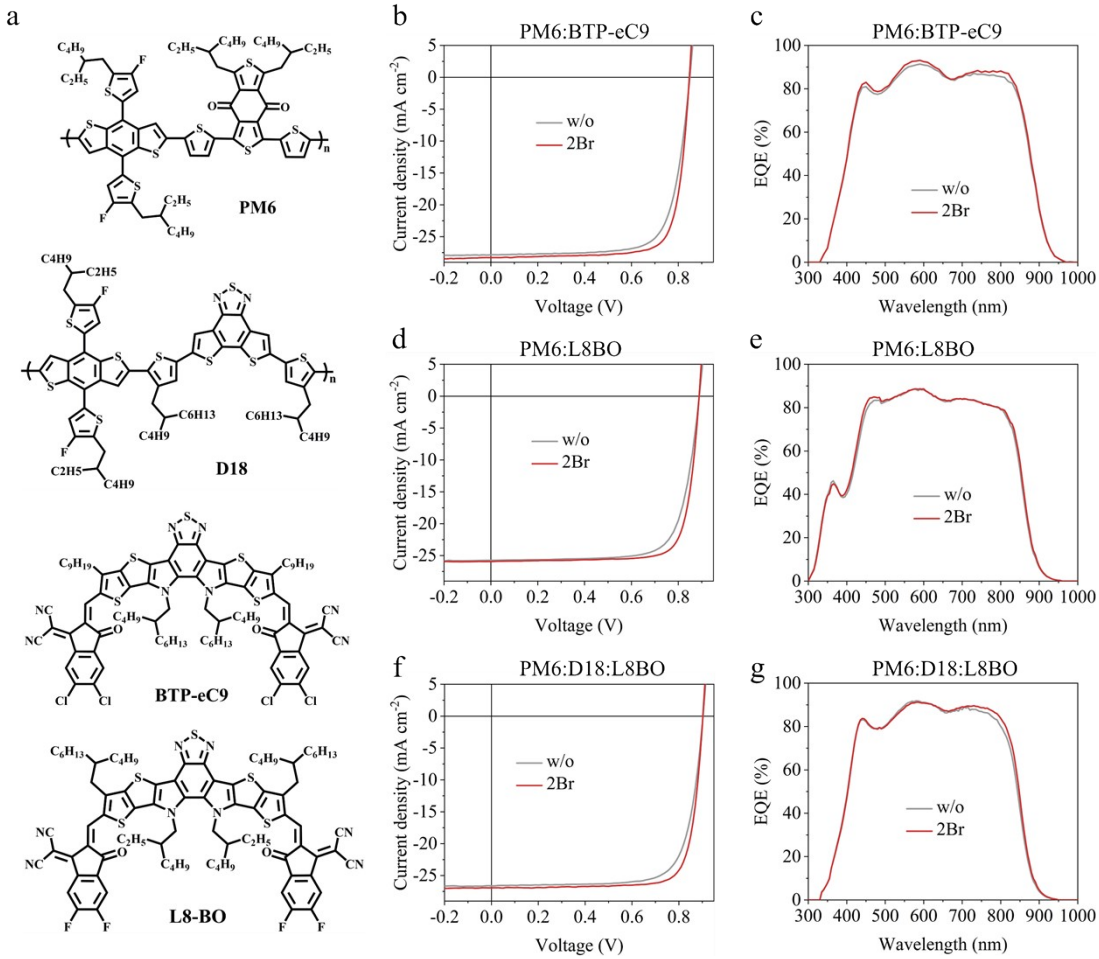

Figure S14. (a) The chemical structure of active layer materials, including PM6, D18, BTP-eC9 and L8BO. *J-V* curves and EQE curves of PM6:BTP-eC9 (b and c), PM6:L8BO (d and e) and PM6:D18:L8BO (f and g) solar cell.

Table S1. The parameters of in-plane (100) and out-of-plane (010) of pristine Y6 and 2Br-processed Y6.

Additive	Peak	q (Å^{-1})	Distance (Å)	FWHM (Å^{-1})	CCL (Å)
w/o	(100)	0.28	22.43	-	-
	(010)	1.65	3.81	0.33	17.13
2Br	(100)	0.28	22.43	-	-
	(010)	1.74	3.61	0.28	20.19

Table S2. The parameters of in-plane (100) and out-of-plane (010) of pristine PM6:Y6 and 2Br-processed PM6:Y6.

Additive	Peak	q (Å^{-1})	Distance (Å)	FWHM (Å^{-1})	CCL (Å)
w/o	(100)	0.28	22.43	-	-
	(010)	1.70	3.69	0.34	16.62
2Br	(100)	0.29	21.66	-	-
	(010)	1.75	3.59	0.32	17.66

Table S3. Photovoltaic parameters of PM6:Y6 device with different contents of additive 2Br.

Contents (%)	V_{oc} (V)	J_{sc} (mA cm^{-2})	FF (%)	PCE (%)
0.3	0.850	26.38	76.31	17.10
0.5	0.849	26.64	77.84	17.60
0.7	0.848	26.50	77.04	17.31
1.0	0.842	26.22	76.79	16.95

Table S4. Device parameters of various active layer with traditional additive CN and DIO.

Active layer	Additive	V_{oc} (V)	J_{sc} (mA cm^{-2})	FF (%)	PCE (%)
PM6:Y6	CN	0.849	26.17	76.33	16.96
	DIO	0.848	26.03	75.53	16.68
PM6:BTP-Ec9	CN	0.845	28.06	77.19	18.29
	DIO	0.843	28.18	77.21	18.34
PM6:L8BO	CN	0.889	25.94	76.31	17.62
	DIO	0.887	25.85	76.45	17.54
PM6:D18:L8BO	CN	0.902	26.91	78.19	18.99
	DIO	0.901	26.78	77.69	18.74

Table S5. The parameters of exciton dissociation and charge collection efficiencies of PM6:Y6 without and with 2Br.

	J_{sc} (mA cm^{-2})	J_{power} (mA cm^{-2})	J_{sat} (mA cm^{-2})	P_{diss} (%)	P_{coll} (%)
w/o	25.84	23.57	26.81	96.4	87.9
2Br	26.64	24.44	27.27	97.7	89.6

Table S6. Photovoltaic parameters of binary PM6:Y6, PM6:BTP-eC9 and PM6:L8BO device with 2Br. Device area is 0.0585 cm^2.

Active layer	Thickness (nm)	V_{oc} (V)	J_{sc} (mA cm^{-2})	FF (%)	PCE (%)
PM6:Y6	100	0.849	26.64	77.84	17.60
	200	0.838	26.31	73.90	16.30
PM6:BTP-Ec9	100	0.847	28.28	78.48	18.80
	200	0.837	27.30	76.36	17.45
PM6:L8BO	100	0.889	25.93	79.67	18.36
	200	0.876	25.86	75.03	17.00

Table S7. Photovoltaic parameters of PM6:D18:L8BO device with 2Br. Device area is 0.0585 cm^2 and module area is 19.3 cm^2.

	Thickness	V_{oc}	J_{sc}/I_{sc} [a]	FF	PCE	Power

	(nm)	(V)	(mA cm^{-2}/mA)	(%)	(%)	(mW)
Device	120	0.903	26.93	80.24	19.51	-
	200	0.895	26.43	76.30	18.05	-
Module	120	6.305	64.05	73.44	15.66	296.59
	200	6.249	63.61	67.34	14.08	267.66

[a] Note that the device uses mA cm^{-2} as the unit of J_{sc}, while the module uses mA as the unit of I_{sc}.

Table S8. The summary of PCEs of the large area modules with different active layer thickness. The module area is more than 18 cm^2.

No.	Area (cm^2)	Thickness (nm)	PCE (%)	Reference
1	19.3	90	16.26	[1]
2	19.3	100	14.79	[2]
3	19.3	100	16.04	[3]
4	36.0	105	14.26	[4]
5	36.0	110	13.47	[5]
6	25.2	110	14.07	[6]
7	25.2	110	14.42	[7]
8	58.5	120	14.04	[8]
9	54.5	130	11.60	[9]
10	18.0	130	14.40	[10]
11	25.0	135	11.29	[11]
12	41.0	143	14.04	[12]
13	20.4	145	10.40	[13]
14	31.5	180	10.77	[14]
15	80.0	200	5.25	[15]
16	20.4	200	9.31	[16]
17	19.3	120	15.66	This work
18	19.3	200	14.08	This work

Reference

[1] T. Chen, X. Zheng, D. Wang, Y. Zhu, Y. Ouyang, J. Xue, M. Wang, S. Wang, W. Ma, C. Zhang, Z. Ma, S. Li, L. Zuo, H. Chen, *Adv. Mater.* **2024**, *36*, 2308061.

[2] J. Fan, Z. Liu, J. Rao, K. Yan, Z. Chen, Y. Ran, B. Yan, J. Yao, G. Lu, H. Zhu, C. Li, H. Chen, *Adv. Mater.* **2022**, *34*, 2110569.

[3] D. Wang, Y. Li, G. Zhou, E. Gu, R. Xia, B. Yan, J. Yao, H. Zhu, X. Lu, H.-L. Yip, H. Chen, C.-Z. Li, *Energy Environ. Sci.* **2022**, *15*, 2629.

[4] H. Chen, R. Zhang, X. Chen, G. Zeng, L. Kobera, S. Abbrent, B. Zhang, W. Chen, G. Xu, J. Oh, S.-H. Kang, S. Chen, C. Yang, J. Brus, J. Hou, F. Gao, Y. Li, Y. Li, *Nat Energy* **2021**, *6*, 1045.

[5] B. Zhang, F. Yang, S. Chen, H. Chen, G. Zeng, Y. Shen, Y. Li, Y. Li, *Adv. Funct. Mater.* **2022**, *32*, 2202011.

[6] X. Dong, Y. Jiang, L. Sun, F. Qin, X. Zhou, X. Lu, W. Wang, Y. Zhou, *Adv. Funct. Mater.* **2022**, *32*, 2110209.

[7] S. Zhang, H. Chen, P. Wang, S. Li, Z. Li, Y. Huang, J. Liu, Z. Yao, C. Li, X. Wan, Y. Chen,

Solar RRL **2023**, *7*, 2300029.

[8] S. Yoon, S. Park, S. H. Park, S. Nah, S. Lee, J.-W. Lee, H. Ahn, H. Yu, E.-Y. Shin, B. J. Kim, B. K. Min, J. H. Noh, H. J. Son, *Joule* **2022**, *6*, 2406.

[9] Z. U. Rehman, M. Haris, S. U. Ryu, M. Jahankhan, C. E. Song, H. K. Lee, S. K. Lee, W. S. Shin, T. Park, J. Lee, *Advanced Science* **2023**, *10*, 2302376.

[10] S. Dong, T. Jia, K. Zhang, J. Jing, F. Huang, *Joule* **2020**, *4*, 2004.

[11] H. Li, S. Liu, X. Wu, Q. Qi, H. Zhang, X. Meng, X. Hu, L. Ye, Y. Chen, *Energy Environ. Sci.* **2022**, *15*, 2130.

[12] X. Lu, C. Xie, Y. Liu, H. Zheng, K. Feng, Z. Xiong, W. Wei, Y. Zhou, *Nat Energy* **2024**, DOI 10.1038/s41560-024-01501-1.

[13] C.-Y. Liao, Y. Chen, C.-C. Lee, G. Wang, N.-W. Teng, C.-H. Lee, W.-L. Li, Y.-K. Chen, C.-H. Li, H.-L. Ho, P. H.-S. Tan, B. Wang, Y.-C. Huang, R. M. Young, M. R. Wasielewski, T. J. Marks, Y.-M. Chang, A. Facchetti, *Joule* **2020**, *4*, 189.

[14] S. Rasool, J. W. Kim, H. W. Cho, Y. Kim, D. C. Lee, C. B. Park, W. Lee, O. Kwon, S. Cho, J. Y. Kim, *Adv. Energy Mater.* **2023**, *13*, 2203452.

[15] Y. W. Han, S. J. Jeon, H. S. Lee, H. Park, K. S. Kim, H. Lee, D. K. Moon, *Adv. Energy Mater.* **2019**, *9*, 1902065.

[16] J. Wu, C. Liao, Y. Chen, R. M. Jacobberger, W. Huang, D. Zheng, K. Tsai, W. Li, Z. Lu, Y. Huang, M. R. Wasielewski, Y. Chang, T. J. Marks, A. Facchetti, *Advanced Energy Materials* **2021**, *11*, 2102648.